



Characterization of Nano-Structured Magnesium-Aluminum Ferrites Synthesized by Citrate-Gel Auto Combustion Method

M. Shahjahan^{1*} , M. A. Bhuyan¹ , M. S. Hossain² ,
M. A. Haque¹ , and D. P. Paul¹ 

¹ Department of Physics, University of Chittagong, Chittagong-4331, Bangladesh.

² Industrial Physics Division, BCSIR Laboratories Dhaka, Bangladesh Council of Scientific & Industrial Research (BCSIR), Dhaka -1205, Bangladesh.

Abstract: An effort is made to find the solution to the new challenges of modification advancements in ferrite technologies. The hypothetical variation in the structural, magnetic, and electrical properties of cubic spinel magnesium aluminum ferrites introduced by the substitution of doping elements has been rationalized and proven. The outcome of aluminum substitution on the magnesium ferrites has been examined and investigated. Spinel ferrites having compositions of $MgAl_xFe_{2-x}O_4$ ($x = 0.1, 0.2, 0.3, 0.4$) were prepared by the sol-gel auto-combustion method. The prepared sample's characterization, such as scanning electron microscopy (SEM), DC electrical resistivity, AC electrical resistivity, and dielectric properties measurements, were tested using the respective instruments. The grain size and crystal size of all samples were measured from the micrographs of SEM and XRD Data. It is found that the average grain size is within the range of 300 nm - 550 nm for all different series that are formed, keeping the samples at 1100 °C sintering temperatures. A two-probe method experiment with a temperature range of 30 °C to 500 °C gives data on DC electrical resistivity. The Curie temperature depends on the sintering temperature, and it increases with increasing doping concentration. Also, doping influences grain size, which decreases with increasing concentration. Analyzing the SEM micrographs, it is found that the average grain size must decrease in tendency with increasing Al content. DC electrical resistivity exhibits excellent semiconducting behavior. Frequency dependence, dielectric constant, and dielectric loss factors were measured, keeping the frequency range of 75 Hz to 130 MHz at room temperature. The result shows that the dielectric constant (ϵ) and dielectric loss tangent (\tan^{TM}) decrease with the increase in frequency, while the AC resistivity and Q-factor increase. Comparing the electrical properties of four compositions, it can be suggested that the mixed ferrite, sample-4 ($x = 0.3$), shows the highest Q-factor of all at 1100 °C.

Keywords: Mg-Al ferrites, sol-gel, nanocrystalline, magnetic properties, electrical properties, DC resistivity, dielectric, loss tangent.

Submitted: April 06, 2023. **Accepted:** July 17, 2023.

Cite this: Shahjahan, M., Bhuyan, M. A., Hossain, M. S., Haque, M. A., & Paul, D. P. (2023). Characterization of Nano-Structured Magnesium-Aluminum Ferrites Synthesized by Citrate-Gel Auto Combustion Method. Journal of the Turkish Chemical Society, Section B: Chemical Engineering, 6(2), 45-62. <https://doi.org/10.58692/jotcsb.127857>.

*Corresponding author. E-mail: shahjahan@cu.ac.bd.

1. INTRODUCTION

Nanoscience and nanotechnology are more attentive to materials and solid-state systems (Joudeh & Linke, 2022) whose components,

structures, and designs exhibit novel and significantly improved physical, chemical, and biological properties because of their nanoscale size (Saini et al., 2010). Research on nano-size technology and nanoparticles has unlocked so

many scopes and versatile uses due to their novel and excellent properties (Sontakke & Purkait, 2021). It also helps create many new materials and use devices with prospective applications, like medicine, toxicity, electronics, and energy production (Buzea et al., 2007). Also, it has an impact on the environment, consumer products, and global economics (Pathania et al., 2021).

Ferrites have remarkable magnetic properties (Ahmed et al., 2022) due to their versatility, low production cost, exclusive electromagnetic performance, high resistivity, low chemical losses, and excellent chemical stability (Hankare et al., 2011) (Amiri et al., 2019) Within a large frequency range (Dixit et al., 2012). Soft ferrites are mostly used in many electrical components, memory-storing devices, microwave functional devices, and magnetic devices because of their high magnetic permeability and low magnetic losses (Lakshmi Ranganatha et al., 2020) (Giannakopoulou et al., 2002). These materials can also be used for different high-temperature procedures because of their strong thermal stability, low electrical conductivity, electrocatalytic activity, and corrosion resistivity (Olsen & Thonstad, 1999). Among these ferrites' techniques, magnesium aluminum ferrites are considered as they showed permeability, resistivity, saturation magnetization, low losses and relatively large Curie temperature (Gimenes et al., 2012). The general formula of magnesium ferrite, $M^{+2}Fe^{+3}_2O_4$ (AB_2O_4), is a type of crystal compound of spinel structure (where M is from the tetrahedral site and Fe from the octahedral site) (Gorter, 1950).

The spinel ferrites have interesting properties to disperse the cations among the tetrahedral (A) and octahedral (B) sites (Bhatu et al., 2007). Substituting non-magnetic and magnetic ions largely affects the ferrite's properties like lattice-related parameters, magnetic moments, and ion exchange interactions (Zakaria et al., 2003) (Zakaria et al., 2004). Scientists use many chemical techniques for the synthesis of ferrites (Giri et al., 2004)(George et al., 2006) (Wang, 2006) (Hankare, Vader, et al., 2009) (Hankare, Sankpal, et al., 2009) (Zhang et al., 1990). The citrate sol-gel auto-combustion process has several advantages, such as nano-scale yield without the use of expensive equipment (Kamble et al., 2013). Because all the reactants are solutions, molecular mixing occurs, and reactant yield can be controlled accurately (Atassi & Tally, 2006). The purpose of the present research is to present a novel and economical method of preparation of Mg-Al ferrites by the sol-gel auto-combustion method.

Doping $MgFe_2O_4$ with metals is the finest method, filled with tetrahedral or octahedral sites that can alter the magnetic, electrical, or structural properties of ferrites. Following the procedure, different properties of ferrites can be engineered to fit a particular application (Shokrollahi, 2008). As per our knowledge, information is not available about the nano-sized Mg-Al ferrites produced using the citrate-gel auto combustion method. Some mixed Cu-Mg-Zn ferrites were synthesized through the co-precipitation method by Bhosale et al. (Kuznetsov et al., 1998) where they found the lattice parameter decreases gradually while density increases with the increase in Mg^{2+} at the substitution level. Qi et al. (Radwan et al., 2003) showed Mn substituted ($Mg_{0.2}Cu_{0.2}Zn_{0.6}O$) ($Fe_{2-x}Mn_xO_3$)_{0.97} ($x = 0.00-0.07$) ferrites using nanosized precursor powders by a sol-gel method and found Mn showed higher initial permeability and good grain morphology than that of NiCuZn ferrites.

It could be a good material for multi-layer chip inductors with high inductance. Nanoparticles of $M_{0.5}Mg_{0.5}Fe_2O_4$ ($M = Ni, Cu, \text{ and } Zn$) are prepared by Pradeep et al. (Lakshman et al., 2005) using the sol-gel method and found greater values of lattice constant of mixed CuZn ferrites. Also, particle size was decreased by the substitution of Cu for Zn. Barati (Arulmurugan et al., 2006) found that properties like initial permeability, saturation magnetization, dielectric constant, and dielectric loss were increased, and AC-resistivity was decreased with the increase in doping contents. Prepared materials may be applicable in multilayer chip inductor applications due to their low loss at high frequencies and good magnetic properties.

In this research, we have prepared nano-ferrites having the composition $MgAl_xFe_{2-x}O_4$ ($x = 0.1, 0.2, 0.3, 0.4$) by the citrate-gel auto combustion method, keeping in mind that the particle size will be small and the magnetic, electrical, and dielectric properties will be improved by the substitution of Fe^{+3} with Al^{+3} ions. According to our knowledge, this is the unique observation of Mg-Al nano-ferrites made using the citrate-gel method with small particle sizes. In this article, we show the citrate gel method-based synthesis, XRD, SEM, EDS, and resistance properties of aluminum-doped magnesium ferrites which will be useful for different purposes.

2. MATERIALS AND METHOD

Mg-Al nano-ferrites using the chemical formula $MgAl_xFe_{2-x}O_4$ ($x = 0.1, 0.2, 0.3, 0.4$) were synthesized by the citrate-gel auto combustion technique using magnesium nitrate hexahydrate ($Mg(NO_3)_2 \cdot 6H_2O$, 99%), iron(II) nitrate nonahydrate ($Fe(NO_3)_2 \cdot 9H_2O$, AR grade), aluminum nitrate

nonahydrate ($\text{Al}(\text{NO}_3)_3 \cdot 9\text{H}_2\text{O}$, AR grade), citric acid ($\text{C}_6\text{H}_8\text{O}_7 \cdot \text{H}_2\text{O}$), AR grade, and ammonia (NH_3 , AR grade). The required amount of nitrate salt and the citric acid solution are formulated using nitrates in a citric acid molar ratio of 1:1. The pH value of the solution is adjusted to 7 with the help of ammonia mixing slowly in the solution. A magnetic hot plate stirrer is used to stir the solution continuously to finish the entire procedure. The solution was poured into a beaker, heated at 100 °C on a hot plate, and stirred continuously till it transformed into a highly viscous gel. All the samples formed as the gel was burned out completely to form a fluffy, loose powder after reaching a proper temperature, starting ignition, and burning in a self-propagating combustion manner. The whole combustion process was done in a short time. Finally, the as-burnt powders were calcinated using the programmable muffle furnace at 500 °C for up to 1 h to get the ferrites of a single phase.

The calcite powders were granulated using a 1% saturated solution of polyvinyl alcohol as a binder and were uniaxially pressed at a fixed pressure up to 0.5 MPa in a stainless-steel die to form pellet specimens of 12 cm diameter. Samples were leveled as sample-1 to sample 4 according to X values. All samples were heated slowly inside the programmable muffle furnace up to 550 °C at a rate of about 2 °C min^{-1} to avoid cracking of the samples. Then, the temperature was raised to 1100 °C, and then the samples were kept at this temperature for 6 h in an airtight atmosphere so that they got cooled slowly inside the furnace. The surfaces of all the specimens were polished to remove oxide and any other extra layer formed during the sintering process.

2.1. Characterization

The structural structure of the synthesized ferrite samples was tested by X-ray diffractometer (XRD) using Cu K_α X-ray radiation ($\lambda=1.5405 \text{ \AA}$) at normal temperature in the angle range of 20° to 85°. X-ray data gives us the phase and crystallite size of the prepared samples, which confirm the formation of a single-phase cubic spinel. Also, the surface morphology and surface features of the prepared ferrites were investigated and recorded by SEM. Dielectric properties, electrical properties, and Curie temperature were investigated by the relevant instruments.

3. RESULTS AND DISCUSSION

3.1. Structural Properties

The X-ray diffraction patterns for the investigated samples have been shown in Figure 1. Powder diffraction by an X-ray powder diffractometer was used to find the crystalline phases using ($\text{Cu-K}\alpha$) = 1.5406 Å at room temperature.

Structural parameters like the lattice parameters and spin phases of all the samples are calculated from the XRD data, and the atomic position of the spinel phases is determined from the literature. All the sharp peaks are in the same position as stated by Giri et al. (2004) which confirmed the sample preparation was accurate and showed a single phase only. The lattice constant is calculated by using the known formula (Iqbal & Siddiquah, 2008)

$$a = d_{hkl} \sqrt{h^2 + k^2 + l^2}$$

Where the Miller indices are h, k, l and interplanar spacing is d_h

It is observed that the highest intensity peak is at the 35.36° position. Calculation gives the peak to be (311), which tells us the prepared samples are spinel ferrites. The average size of the crystal bulk sample (D_p) is calculated using the Scherrer equation (Patterson, 1939)

$$D_p = \frac{0.94 \lambda}{\beta \cos \theta}$$

Where the line broadening in radians is β , Bragg angle is θ , and the X-ray wavelength is λ .

Data showed that the crystal size reduces with a decrease in Fe content as it is larger than the Al atoms, as shown in Table 1. From the table data, it is observed that the lattice constant is almost the same for all samples but tends to be larger as the concentration of cations increases in every sample. Also, we have calculated the X-ray density using the formula (Krishna et al., 2012a)

$$\rho_{\text{ferrite}} = \sum \frac{8M}{Na^3}$$

Here, M is the molecular weight of the sample, Avogadro's number is N , and the lattice constant is a .

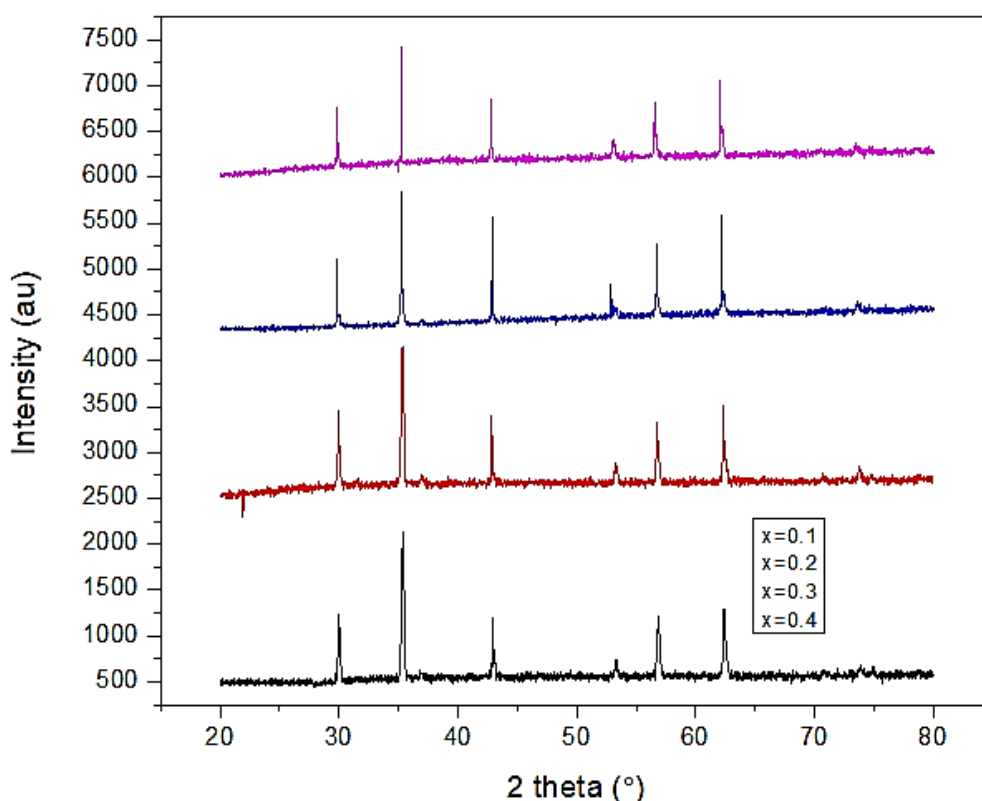


Figure 1: XRD patterns for $\text{MgAl}_x\text{Fe}_{2-x}\text{O}_4$ ferrites. $x = 0.1$ (purple), 0.2 (blue), 0.3 (red), 0.4 (black).

The actual physical bulk density of the tablet shaped prepared ferrites sample was calculated using the formula (Sujatha et al., 2013)

$$d_{\text{bulk}} = \frac{m}{\pi r^2 t}$$

Here, mass is m , the pellet radius is r , and t is the thickness of the sample. Applying the Archimedeian porosimetry theory, the percentage of porosity (%P) is calculated and shown in Table 1. It was also observed that the porosity from the SEM micrographs manually got a similar result. Observing the lattice constant, a decreasing trend is due to the increase in Al content and the decrease in Fe content. Sample -1 ($x=0.1$) showed the highest bulk density, which means porosity would be lower due to high density and is observed accordingly, as shown in Table 1,

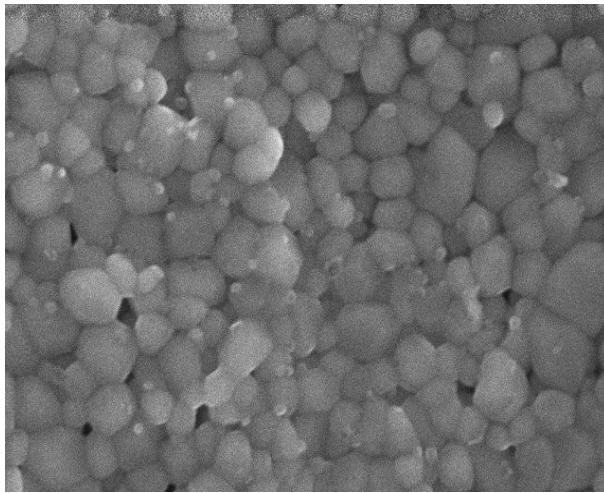
The bulk density of the ferrite samples decreases gradually with the decrease in the Fe^{2+}

concentration as the large atomic weight of Fe is compared with the Mg atoms shown in Table 1. High porosity is observed in the sample 4 ($x=0.4$) which is lowest density sample. Bulk density is decreased due to a decrease in Fe content, and Al concentration improves the magnification, which decreases the porosity.

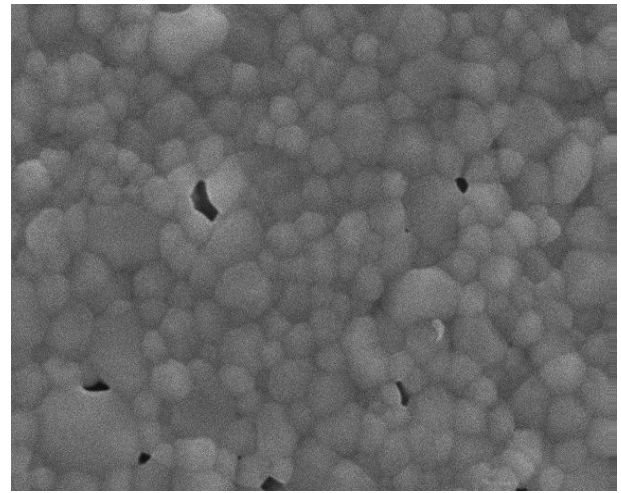
Also, the table showed that the X-ray density calculated has a reducing tendency with the higher Al concentration shown and shows an inverse relation with lattice parameters. Barati et al. got the same result (Giri et al., 2004). It is observed here that, there is a correlation and closed agreement between the theoretical X-ray densities, the observed bulk density, and the porosity of the sintered ferrites. Due to the pore in the sample, X-ray densities are larger than bulk densities. This close relationship with such parameters of ferrites indicated good quality ferrites.

3.2. Morphology by SEM

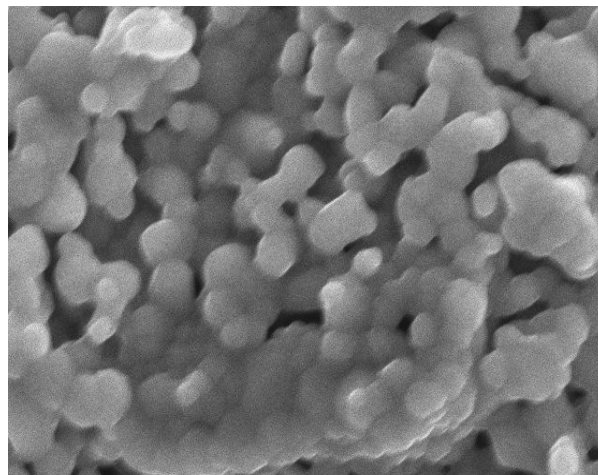
SEM representative micrographs of the samples with different amounts of substitution are shown in Figure 2.



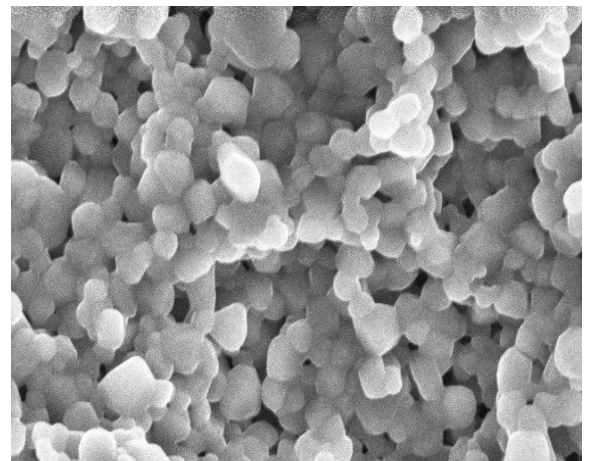
Sample 1



Sample 2



Sample 3



Sample 4

Figure 2: SEM micrographs of various compositions.

Images were taken at different magnifications. The images showed large agglomerates of strongly connected cubic aggregates and well-defined particles of the powder sample with an inhomogeneous, broader grain size distribution. Mechanically activated nano-sized particles showed this type of broader size distribution. (Oñoro et al., 2021)

This agglomeration is caused by the interaction of nano-sized magnetic fine particles with a permanent magnetic moment proportional to their volume. Hence, agglomeration results from the contribution of the permanent magnetization

property of each particle (Arulmurugan et al., 2006). The foam-like structure is found in the porous network of sintered bodies. It is assumed that magnesium ions influence ferrite formation; hence, the compound formation showed the least mass. From the SEM micrographs, we also found that the particle size of the sample is in the nanometer range. We found a trend that, with an increase in Al composition, the grain size in the crystal decreased moderately.

3.3. Composition Dependent DC Electrical Properties

DC electrical resistivity is used to understand the conductivity of the prepared sample. It is measured using the two probe electrical method. A fixed voltage was applied across the sample holder, keeping the sample in series and the standard resistance lower than the sample resistance. The voltage dropped across the resistance was measured using a voltmeter, and the current was measured using an ampere meter. Using the voltage and current across the sample, resistivity is calculated using the relation

$$R = RA/l \quad \Omega\text{-cm} \quad (\text{Krishna et al., 2012b})$$

Where, R_f : Fixed Resistance; A : Surface area of the sample $= \pi r^2$; l : Thickness of the sample; R is the resistance of the sample, and it is given by $R = (V_s/V_f) \times R_f$. Hence, from the above equations, $r = AR_f/l (V_s/V_f)$, V_s is the voltage across the sample, V_f is the voltage across the fixed resistance.

The DC resistivity of the sample was found to increase at a normal temperature from $0.81 \times 10^6 \Omega\text{-cm}$ to $1.85 \times 10^6 \Omega\text{-cm}$ and at transition point from $0.39 \times 10^6 \Omega\text{-cm}$ to $2.0 \times 10^6 \Omega\text{-cm}$ with increasing Al^{3+} from $x = 0.1$ to $x = 0.4$, as mentioned in Table 2.

The DC resistivity ($\ln\rho$) vs. temperature ($1000/T$) curve for all samples at $1100 \text{ }^\circ\text{C}$ has been plotted as shown in Figure 3. From the figure, we found that the DC resistivity has a common trend for all samples and decreases sharply with increasing temperature up to a transition point. After that temperature, the resistivity decreases with increasing temperature slowly and almost constant after a certain time. The resistivity of all samples shows similar characteristics, but the values of resistivity increase with an increase in the Al concentration, as shown in Table 2. In this case, the Curie temperature, T_c , is found to be $115 \text{ }^\circ\text{C}$, $125 \text{ }^\circ\text{C}$, $135 \text{ }^\circ\text{C}$, and $140 \text{ }^\circ\text{C}$, respectively, for all samples.

The increase in resistivity might be due to Al concentration increases, while Fe^{3+} concentration decreases for their occupation on octahedral sites, which is produced during sintering (Islam et al.,

2004). The activation energy (E_p) increases with the increase in Al content. It increases up to $x = 0.3$ but again reduces for $x = 0.4$. This is due to the Al ions. For many ions, some ions may not participate in the reaction, and the activation energy goes lower. Also, Al concentration has an effect on Curie temperature and shifts it to a higher temperature. Another reason for the increase in ρ with increasing Al composition is that Mg^{2+} ions tend to occupy the tetrahedral sites (A) and Al ions choose to go to the octahedral sites (B). Also, Fe ions partially occupy both A and B sites, which increases temperature and decreases conductivity, and hence resistivity increases which confirms that the prepared ferrite under this research has semiconductor-like properties.

Also, Figure 4 indicates the resistivity variation with the ferrite's composition. It is observed that the resistivity is not linear. At $x = 0.3$, resistivity graphs showed slight variation, meaning if Al concentration increases, resistivity decreases slowly and then increases again.

3.4. Effect of Al Concentration Variation on AC Resistivity

The electrical measurements are performed for all Mg-Al ferrite samples at room temperature within the frequency ranges from 75 kHz to 2 MHz using an LCR-Q meter. This is the resistance (R_p in $\text{K}\Omega$) of the sample that was obtained by changing the input frequencies.

The AC resistivity is easily calculated by using ohm's law, $R = \rho \frac{l}{A}$ or $\rho = \frac{RA}{l}$ where R is the resistance of the sample, ρ is the resistivity of the sample, l is the thickness of the specimen or sample, and A is the area of the sample or specimen. The AC conductivity can therefore be determined as follows: $\Sigma_{a.c.} = 1/\rho$. Figure 5 of AC resistivity reveals that the observed samples have low conducting behavior, which increases with frequency. Among the frequency range, conductivity is high in the low-frequency region, and after that, it is moderately frequency-dependent. As the Al content of the sample increases, the conductivity becomes frequency independent, and a line is observed.

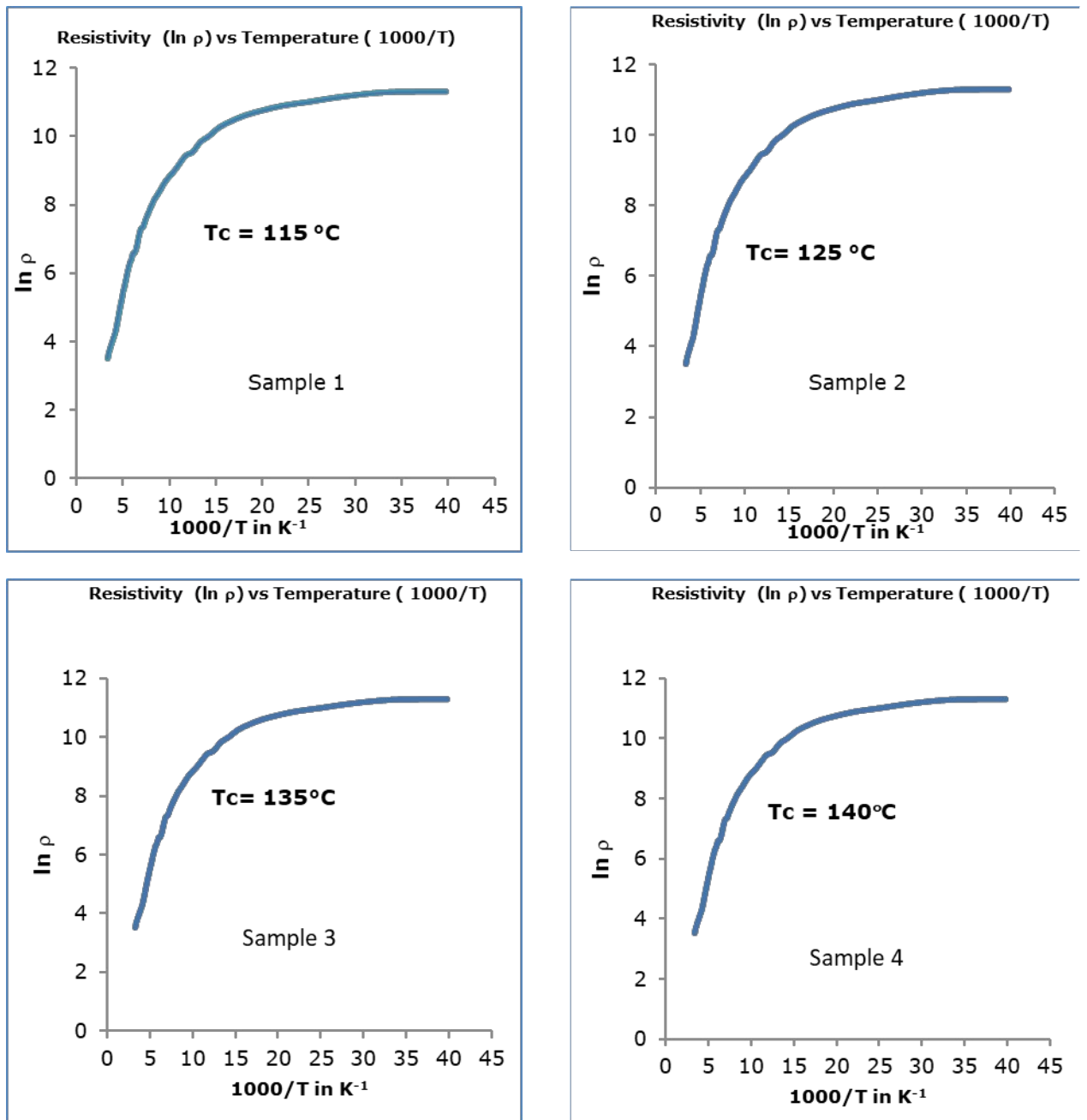


Figure 3: DC Resistivity ($\ln \rho$) Vs. Temperature ($1000/T$) curve for all samples.

Table 1: The structural parameters measured from the XRD graphs.

Sample Composition	FWHM	Crystallite size (nm)	Crystal Strain	Lattice constant (Å)	X-Ray density (r_x)(gcm ⁻³)	Bulk density (r_a) (gcm ⁻³)	% (P)
MgAl _{0.1} Fe _{1.9} O ₄	0.2131	40.31	0.0035	8.4086	4.3826	4.9424	8.62
MgAl _{0.2} Fe _{1.8} O ₄	0.2458	34.95	0.0040	8.4188	4.3232	4.7713	11.35
MgAl _{0.3} Fe _{1.7} O ₄	0.2599	33.05	0.0043	8.4174	4.2611	4.5482	10.83
MgAl _{0.4} Fe _{1.6} O ₄	0.2676	32.1	0.0044	8.4098	4.2082	4.3485	11.16

Table 2: Different parameters of Mg-Al ferrites for temperature 1100° C.

Sample Composition	X	Average grain size, L(nm)	Resistivity, r in Ω-m at room temperature	Transition temperature T _c (°C)	Resistivity r in Ω-m at T _c	Activation Energy (eV) *10 ⁻²
MgAl _{0.1} Fe _{1.9} O ₄	0.1	436	81181.38	115	3967.97	234
MgAl _{0.2} Fe _{1.8} O ₄	0.2	300	132336.8	125	7464.56	257
MgAl _{0.3} Fe _{1.7} O ₄	0.3	365	171720	135	10442.97	255
MgAl _{0.4} Fe _{1.6} O ₄	0.4	516	185563.1	140	20555.3	248

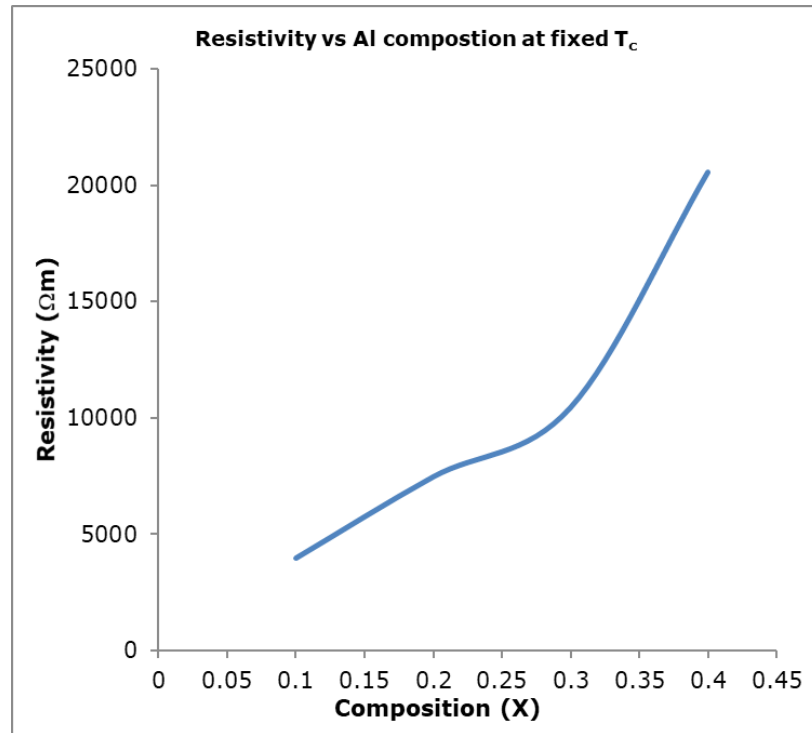


Figure 4: Variation of resistivity with all compositions.

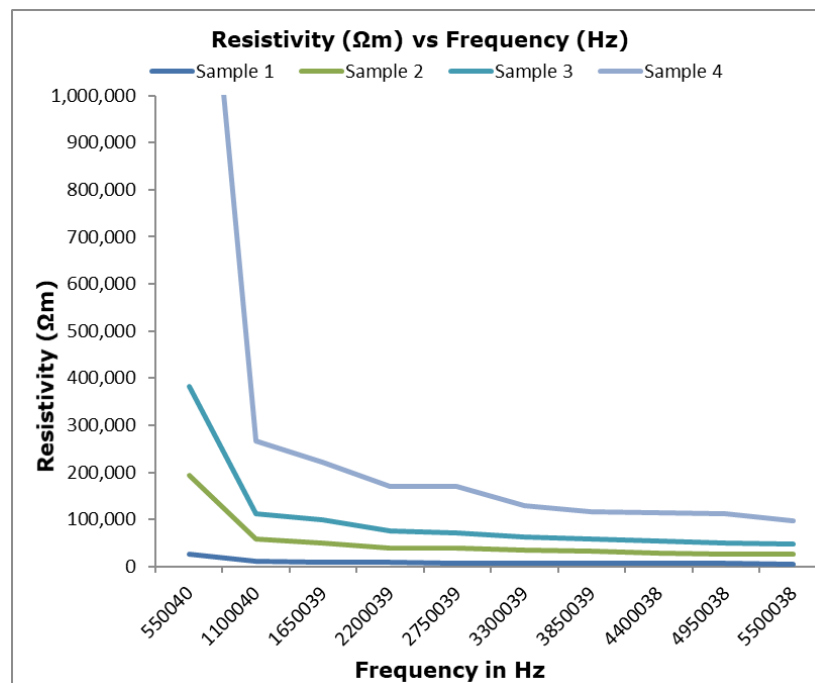


Figure 5: Resistivity (Ωm) vs Frequency (Hz) for all samples.

Figures 5 and 6 show how the amount of Al doping affects the resistivity and AC conductivity of different kinds of Mg-Al ferrites at 1100 °C as a function of frequency.

The values of AC resistivity depend on frequency and show a decreasing tendency with frequency

for all samples; hence, AC conductivity has an increasing tendency. Resistivity graphs are identical in shape, but for samples 3, 4, and 5, they decrease more rapidly than 1 and 2 after a certain frequency. But the AC conductivity is going to be maximum for sample 4, and the other 3 samples have a similar pattern.

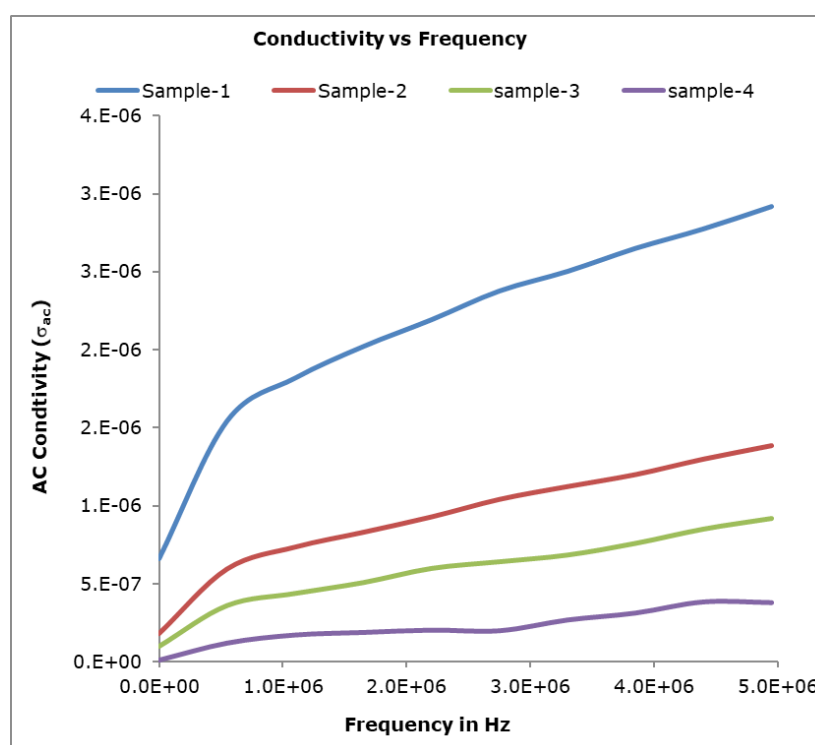


Figure 6: AC conductivity (σ_{AC}) vs Frequency (Hz) for all samples.

3.5. Curie temperature (T_c)

The Curie temperature, or magnetic transition point, gives considerable information about the magnetic states of the substance. It has been determined from the graph of the resistivity as a function of temperature, as shown in Figure 2. It showed a slope at a fixed temperature point, which indicates the transition of the sample from ferrimagnetism to paramagnetism. The Curie temperature is presented for all samples in Table 1, and a graph is presented in Figure 7. It showed that Curie temperature changes with the Al concentration present in the sample and has an increasing tendency from 115 °C to 140 °C with increases in Al^{3+} composition from $x = 0.1$ to 0.4.

3.6. Activation Energy

Using the electrical data, we have calculated the activation energies of ferrites and paramagnetic regions by following the formula $\rho = \rho_0 \exp$

$(E_p/K_B T_c)$ used by Bhise et al, Patil et al, Snelling and others (Gu, 2003) and graphs of $\ln \rho$ versus $1000/T$ slope are given in Table 1. Here, ρ_0 is the resistivity at $t = 0$ °C. E_p is the activation energy. K_B is the Boltzmann constant. We found that at the 115 °C transition temperature (T_c), the activation energy is 0.0234 eV/K. It decreases from 0.0234 eV to 0.0248 eV as the Al^{3+} composition increases from $x = 0.1$ to 0.4. Also, it varies with composition, as shown in Figure 8. It has a decreasing trend, which may be due to a lack of oxygen vacancies (Kuznetsov et al., 1998).

Also, resistivity decreases with increasing Al^{3+} concentration because activation energy acts like DC electrical resistivity (Radwan et al., 2003). Activation energy is getting smaller, representing the electrons hopping among the ions of different valences. The gradual decrease of conductivity calculated at 1 kHz, excluding sample 1, with

increasing Al content shown in Table 1 can cause a decrease in the total number of charge carriers (Willey et al., 1993). Here, we also observed from

the figure that the activation energy is inversely proportional to the conductivity as well as to the ferrite's composition.

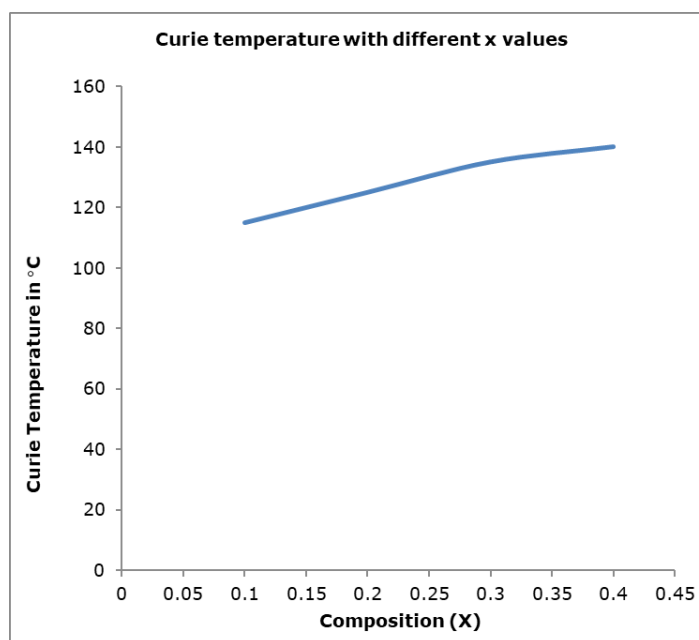


Figure 7: Variation of Curie temperature with composition.

Table 3: AC electrical properties measurements for four Mg-Al ferrites samples.

Sample No	Dielectric constant (ϵ)		Dielectric loss tangent ($\tan\delta$)		Q-factor at frequency		Resistivity ρ Ωm	
	5.5E+5	1.10E+7	5.5E+5	1.10E+7	5.5E+5	1.10E+7	5.5E+5	1.10E+7
at (1100°C)	5	+7	Hz	7	Hz	7	Hz	Hz
	Hz	Hz		Hz		Hz		
X=0.1	5.45	4.85	0.32	0.0097	0.0064	100.23	3.24E+4	3.5E+4
X=0.2	6.81	5.55	0.648	0.048	0.0023	20.7	1.09E+4	6.3E+3
X=0.3	7.37	6.6	0.291	0.0069	0.00571	147.3	2.7E+4	3.52E+4
X=0.4	6.25	5.48	0.3	0.011	0.02	86.8	1.7E+5	3.5E+4

Table 3 showed the numeric values of Dielectric constant (ϵ), Dielectric loss tangent ($\tan\delta$), Q-factor and Resistivity of all samples at different temperatures at frequencies of 5 MHz and 110 MHz

3.7. Effect of Al concentration on dielectric constant, loss tangent and Q factor

The electrical measurements were performed on four samples at room temperature for the

frequency ranges from 75 kHz to 2 MHz using an LCR-Q meter. We obtained the values of capacitances (C_p in μF) by changing the frequencies. Using this data, dielectric constants were measured using the following formula: $\epsilon = C_p / \epsilon_0 A$. Where ϵ is the dielectric constant, C_p is the capacitance of the sample, l is the thickness of the specimen or sample, A is the area of the sample or specimen and ϵ_0 is the permittivity of the free space. In our present investigation, we have also determined the Q-factor, the dielectric

constant, and the dielectric loss tangent with the help of an LCR-Q meter.

The Dielectric constant has a variation with composition at 100 kHz, as shown in Figure 9. Here, we observed that the dielectric constant increases with increasing Al concentration, which may contribute to the exchange between Fe^{2+3} and Fe^{3+} ions. This creates the chance to increase the polarization and dielectric constant (Willey et al., 1993). From the figure, it is observed that the dielectric constant decreases with increasing

frequency and ultimately reaches a fixed value. It is because polarization decreasing with frequency is a common trend for dielectric constant.

The observed nanostructural features have a major influence on the dielectric properties of doped Mg-Al ferrites. The value of the dielectric constant depends on the frequency and increases with an increase in Al content. But it showed a significant difference for all samples; this is due to low-temperature synthesis. After a certain frequency, the dielectric constant increases again.

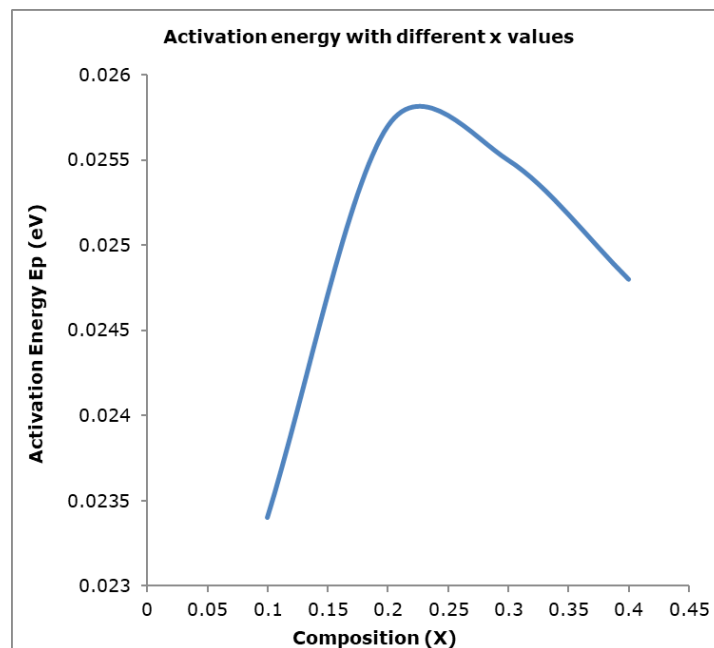


Figure 8: Variation of activation energy with composition.

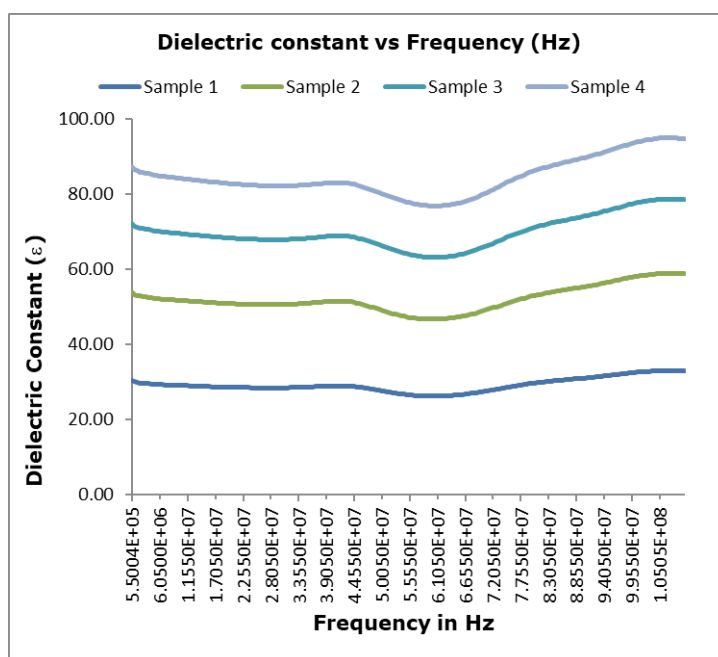


Figure 9: Dielectric constant vs Frequency (Hz) for all samples.

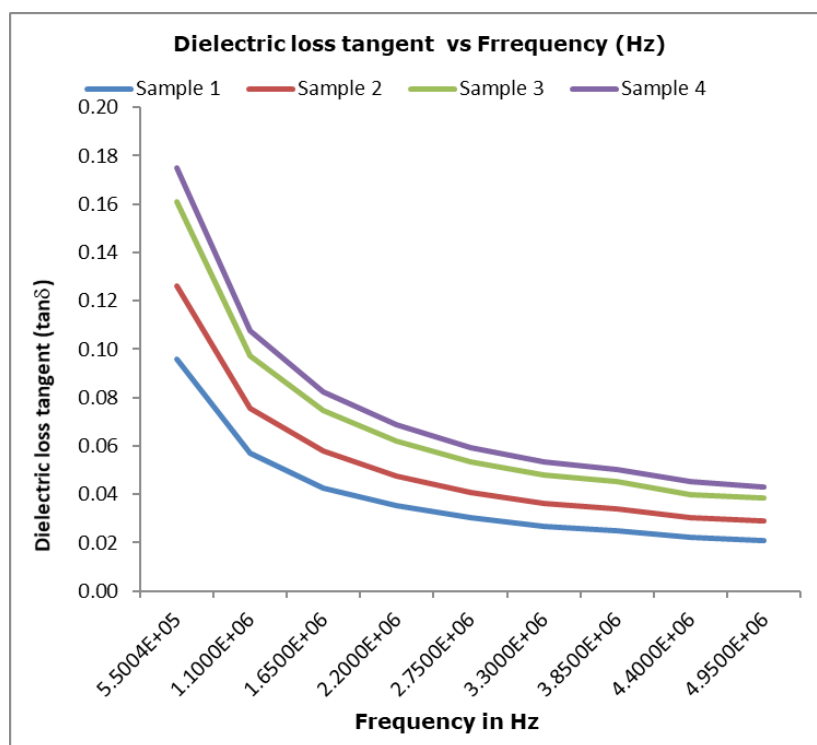


Figure 10: Dielectric loss tangent (tan δ, Y axis) vs (Hz, X axis) for all samples.

The loss factor decreases from 1.8 to 0.02 with the increase in frequency from 0.55 MHz to 4.9 MHz, as shown in Figure 10. The dielectric loss tangent (tanδ) basically depends on stoichiometry, Fe²⁺ content, and structural homogeneity, which again depend on

compositional content and sintering temperature. The dielectric loss tangent vs. frequency graph for all samples showed that the dielectric loss tangent decreased with increasing frequency.

According to Iwachi (Oñoro et al., 2021), the conduction mechanism and the dielectric of ferrites have a strong correlation. When the hopping frequency is approximately equal to the externally applied electric field frequency, the loss tangent is highest. It is shown that the dielectric

loss tangent of sample 1 is high. The hopping frequencies are observed with a maximum loss at 0.55 MHz and a minimum loss of 11.36 MHz. The hopping of electrons between Fe^{2+} and Fe^{3+} plays the role of a conduction mechanism.

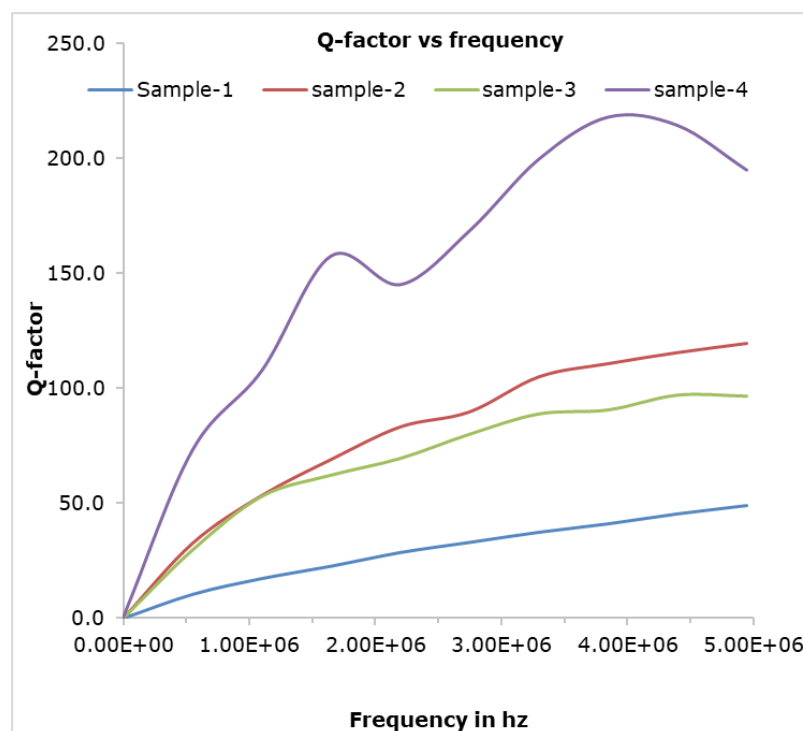


Figure 11: Quality factor (Q-factor, Y axis) Vs. Frequency (Hz, X axis) for all samples.

The quality factor (Q-factor) vs. frequency is presented in Figure 11. From the graph, it is observed that the Q-factor has an increasing tendency with the increasing frequency of the applied frequency. Sample 4 showed the highest Q-factor, but the response to the frequency is not linear, as the curve itself is a zigzag path. The other three samples had the same Q-factor response, and sample 2 showed the highest Q-factor.

4. CONCLUSION

Maintaining proper deposition conditions and using the chemical formula $\text{MgAl}_x\text{Fe}_{2-x}\text{O}_4$ with traces of some additives are reported. The sol-gel autocombustion and formation reaction method has been adopted and applied to prepare the investigated ferrites.

Al substitution for ferrites brought remarkable changes in the structural, electrical, and magnetic properties. XRD spectra supported the formation of spinel ferrites and other crystal

information, including crystal size and shape. From the XRD spectra, the crystal size is calculated at about 30–40 nm. SEM analysis indicates that the ferrites have the expected homogeneity and uniform morphology. It is found that the grain size has an increasing tendency according to the increase in Al ion concentration.

Also, some new nuclei were formed and observed, which is responsible for preventing further grain growth, and it is assumed that the grain size decreased due to this. The DC resistivity increases up to the transition temperature of 115 °C and then decreases. The SEM image gives an idea of substitution's effect on grain size and grain distribution. Comparing the X-ray density and bulk density data demonstrates that all the samples are slightly porous and have a consistent density.

Also, increasing the Al concentration will increase the dielectric constant. The dielectric loss factor decreases largely from 19.82 to 0.481 with the increase in frequency from 80 Hz to 1 M Hz. The

resistivity decreases with frequency, but after $5.5E+6$ (Hz), it will increase again. The AC resistivity is also frequency-dependent and decreases with frequency. A sample with composition $x = 0.4$ has a higher value of the Curie temperature. Hence, the materials are suitable for use in the frequency range of 10-1000 kHz.

5. ACKNOWLEDGEMENTS

We would like to express our grateful thanks and gratitude to the authorities of the University of Chittagong and BCSIR Laboratories, Dhaka for providing us the opportunity and the necessary permission to carry out this research work. Thanks, are also due to all the employees of the department of Physics, University of Chittagong and Industrial Physics Division at BCSIR Laboratories, Dhaka.

6. REFERENCES

- Ahmed, M., Hossain, M. D., Akter, S., Hossain, M. A., Sikder, S. S., Hakim, M. A., & Khan, M. N. I. (2022). Structural and magnetic properties of $Co_{0.85}Zn_{0.15}YxFe_{2-x}O_4$ ferrites. *Physica B: Condensed Matter*, 645, 414267. <https://doi.org/10.1016/j.physb.2022.414267>
- Amiri, M., Salavati-Niasari, M., & Akbari, A. (2019). Magnetic nanocarriers: Evolution of spinel ferrites for medical applications. *Advances in Colloid and Interface Science*, 265, 29-44. <https://doi.org/10.1016/j.cis.2019.01.003>
- Arulmurugan, R., Vaidyanathan, G., Sendhilnathan, S., & Jeyadevan, B. (2006). Mn-Zn ferrite nanoparticles for ferrofluid preparation: Study on thermal-magnetic properties. *Journal of Magnetism and Magnetic Materials*, 298(2), 83-94. <https://doi.org/10.1016/j.jmmm.2005.03.002>
- Atassi, Y., & Tally, M. (2006). Low sintering temperature of Mg-Cu-Zn ferrite prepared by the citrate precursor method. *Journal of the Iranian Chemical Society*, 3(3), 242-246. <https://doi.org/10.1007/BF03247214>
- Bhatu, S. S., Lakhani, V. K., Tanna, A. R., Vasoya, N. H., Buch, J. U., Sharma, P. U., Trivedi, N., Joshi, H. H., & Modi, K. B. (2007). Effect of nickel substitution on structural, infrared and elastic properties of lithium ferrite. In *Indian Journal of Pure & Applied Physics* (Vol. 45).
- Buzea, C., Pacheco, I. I., & Robbie, K. (2007). Nanomaterials and nanoparticles: Sources and toxicity. *Biointerphases*, 2(4), MR17-MR71. <https://doi.org/10.1116/1.2815690>
- Dixit, G., Singh, J. P., Srivastava, R. C., Agrawal, H. M., & Chaudhary, R. J. (2012). Structural, Magnetic And Optical Studies Of nickel Ferrite Thin Films. *Advanced Materials Letters*, 3(1), 21-28. <https://doi.org/10.5185/amlett.2011.6280>
- George, M., Mary John, A., Nair, S. S., Joy, P. A., & Anantharaman, M. R. (2006). Finite size effects on the structural and magnetic properties of sol-gel synthesized $NiFe_{2}O_4$ powders. *Journal of Magnetism and Magnetic Materials*, 302(1), 190-195. <https://doi.org/10.1016/j.jmmm.2005.08.029>
- Giannakopoulou, T., Kompotiatis, L., Kontogeorgakos, A., & Kordas, G. (2002). Microwave behavior of ferrites prepared via sol-gel method. *Journal of Magnetism and Magnetic Materials*, 246(3), 360-365. [https://doi.org/10.1016/S0304-8853\(02\)00106-3](https://doi.org/10.1016/S0304-8853(02)00106-3)
- Gimenes, R., Baldissera, M. R., da Silva, M. R. A., da Silveira, C. A., Soares, D. A. W., Perazolli, L. A., da Silva, M. R., & Zaghete, M. A. (2012). Structural and magnetic characterization of $MnxZn_{1-x}Fe_2O_4$ ($x=0.2; 0.35; 0.65; 0.8; 1.0$) ferrites obtained by the citrate precursor method. *Ceramics International*, 38(1), 741-746. <https://doi.org/10.1016/j.ceramint.2011.07.066>
- Giri, J., Sriharsha, T., & Bahadur, D. (2004). Optimization of parameters for the synthesis of nano-sized $Co_{1-x}Zn_xFe_2O_4$, ($0 \leq x \leq 0.8$) by microwave refluxing. *J. Mater. Chem.*, 14(5), 875-880. <https://doi.org/10.1039/B310668C>
- Gorter, E. W. (1950). Magnetization in Ferrites: Saturation Magnetization of Ferrites with Spinel Structure. *Nature*, 165(4203), 798-800. <https://doi.org/10.1038/165798a0>
- Gu, B. X. (2003). Magnetic properties and magneto-optical effect of $Co_{0.5}Fe_{2.5}O_4$ nanostructured films. *Applied Physics*

- Letters*, 82(21), 3707–3709.
<https://doi.org/10.1063/1.1573357>
- Hankare, P. P., Patil, R. P., Garadkar, K. M., Sasikala, R., & Chougule, B. K. (2011). Synthesis, dielectric behavior and impedance measurement studies of Cr-substituted Zn-Mn ferrites. *Materials Research Bulletin*, 46(3), 447–452.
<https://doi.org/10.1016/j.MATERRESBULL.2010.11.026>
- Hankare, P. P., Sankpal, U. B., Patil, R. P., Mulla, I. S., Lokhande, P. D., & Gajbhiye, N. S. (2009). Synthesis and characterization of $\text{CoCr}_x\text{Fe}_{2-x}\text{O}_4$ nanoparticles. *Journal of Alloys and Compounds*, 485(1-2), 798–801.
<https://doi.org/10.1016/j.jallcom.2009.06.087>
- Hankare, P. P., Vader, V. T., Patil, N. M., Jadhav, S. D., Sankpal, U. B., Kadam, M. R., Chougule, B. K., & Gajbhiye, N. S. (2009). Synthesis, characterization and studies on magnetic and electrical properties of Mg ferrite with Cr substitution. *Materials Chemistry and Physics*, 113(1), 233–238.
<https://doi.org/10.1016/j.matchemphys.2008.07.066>
- Iqbal, M. J., & Siddiquah, M. R. (2008). Electrical and magnetic properties of chromium-substituted cobalt ferrite nanomaterials. *Journal of Alloys and Compounds*, 453(1-2), 513–518.
<https://doi.org/10.1016/j.jallcom.2007.06.105>
- Islam, M. U., Abbas, T., Niazi, S. B., Ahmad, Z., Sabeen, S., & Chaudhry, M. A. (2004). Electrical behaviour of fine particle, co-precipitation prepared Ni-Zn ferrites. *Solid State Communications*, 130(5), 353–356.
<https://doi.org/10.1016/j.ssc.2004.02.019>
- Joudeh, N., & Linke, D. (2022). Nanoparticle classification, physicochemical properties, characterization, and applications: a comprehensive review for biologists. *Journal of Nanobiotechnology*, 20(1), 262.
<https://doi.org/10.1186/s12951-022-01477-8>
- Kamble, S. S., Jagtap, V. S., & Pingale, P. C. (2013). Synthesis of $\text{Mg}_{0.48}\text{Cu}_{0.12}\text{Zn}_{0.40}\text{Fe}_2\text{O}_4$ ferrite and its aptness for multilayer chip component application. *Ceramics International*, 39(4), 3597–3601.
<https://doi.org/10.1016/j.ceramint.2012.10.187>
- Krishna, K. R., Kumar, K. V., & Ravinder, D. (2012a). Structural and Electrical Conductivity Studies in Nickel-Zinc Ferrite. *Advances in Materials Physics and Chemistry*, 02(03), 185–191.
<https://doi.org/10.4236/ampc.2012.23028>
- Kuznetsov, M. V., Pankhurst, Q. A., & Parkin, I. P. (1998). Self propagating high-temperature synthesis of chromium substituted magnesium zinc ferrites $\text{Mg}_{0.5}\text{Zn}_{0.5}\text{Fe}_{2-x}\text{Cr}_x\text{O}_4$ ($0 \leq x \leq 1.5$). *Journal of Materials Chemistry*, 8(12), 2701–2706.
<https://doi.org/10.1039/a804942d>
- Lakshman, A., Rao, P. S. V. S., Rao, B. P., & Rao, K. H. (2005). Electrical properties of In^{3+} and Cr^{3+} substituted magnesium-manganese ferrites. *Journal of Physics D: Applied Physics*, 38(5), 673–678.
<https://doi.org/10.1088/0022-3727/38/5/002>
- Lakshmi Ranganatha, V., Pramila, S., Nagaraju, G., Udayabhanu, Surendra, B. S., & Mallikarjunaswamy, C. (2020). Cost-effective and green approach for the synthesis of zinc ferrite nanoparticles using Aegle Marmelos extract as a fuel: catalytic, electrochemical, and microbial applications. *Journal of Materials Science: Materials in Electronics*, 31(20), 17386–17403. <https://doi.org/10.1007/s10854-020-04295-6>
- Olsen, E., & Thonstad, J. (1999). Nickel ferrite as inert anodes in aluminium electrolysis: Part II Material performance and long-term testing. *Journal of Applied Electrochemistry*, 29(3), 301–311.
<https://doi.org/10.1023/A:1003464304488>
- Oñoro, M., Macías-Delgado, J., Auger, M. A., Hoffmann, J., de Castro, V., & Leguey, T. (2021). Powder Particle Size Effects on Microstructure and Mechanical Properties of Mechanically Alloyed ODS Ferritic Steels. *Metals*, 12(1), 69.
<https://doi.org/10.3390/met12010069>
- Pathania, A., Kumar, R., Rojhe, K., Goel, B., Aggarwal, S., & Mahto, D. (2021). Value stream mapping – Panacea for lead time reduction in ferrite core industry. *Materials Today: Proceedings*, 46, 2456–2461.

- <https://doi.org/10.1016/j.matpr.2021.01.362>
- Patterson, A. L. (1939). The Scherrer Formula for X-Ray Particle Size Determination. *Physical Review*, 56(10), 978-982.
<https://doi.org/10.1103/PhysRev.56.978>
- Radwan, F. A., Ahmed, M. A., & Abdelatif, G. (2003). Screening effect of Ti⁴⁺ ions on the electrical conductivity and thermoelectric power of Mg ferrite. *Journal of Physics and Chemistry of Solids*, 64(12), 2465-2477.
<https://doi.org/10.1016/j.jpcs.2003.08.003>
- Saini, R., Saini, S., & Sharma, S. (2010). Nanotechnology: the future medicine. *Journal of Cutaneous and Aesthetic Surgery*, 3(1), 32-33.
<https://doi.org/10.4103/0974-2077.63301>
- Shokrollahi, H. (2008). Magnetic properties and densification of Manganese-Zinc soft ferrites (Mn_{1-x}Zn_xFe₂O₄) doped with low melting point oxides. *Journal of Magnetism and Magnetic Materials*, 320(3-4), 463-474.
<https://doi.org/10.1016/j.jmmm.2007.07.003>
- Sontakke, A. D., & Purkait, M. K. (2021). A brief review on graphene oxide Nanoscrolls: Structure, Synthesis, characterization and scope of applications. *Chemical Engineering Journal*, 420, 129914.
<https://doi.org/10.1016/j.cej.2021.129914>
- Sujatha, Ch., Venugopal Reddy, K., Sowri Babu, K., RamaChandra Reddy, A., & Rao, K. H. (2013). Effect of sintering temperature on electromagnetic properties of NiCuZn ferrite. *Ceramics International*, 39(3), 3077-3086.
<https://doi.org/10.1016/j.ceramint.2012.09.087>
- Wang, J. (2006). Prepare highly crystalline NiFe₂O₄ nanoparticles with improved magnetic properties. *Materials Science and Engineering: B*, 127(1), 81-84.
<https://doi.org/10.1016/j.mseb.2005.09.003>
- Willey, R. J., Noirclerc, P., & Busca, G. (1993). PREPARATION AND CHARACTERIZATION OF MAGNESIUM CHROMITE AND MAGNESIUM FERRITE AEROGELS. *Chemical Engineering Communications*, 123(1), 1-16.
<https://doi.org/10.1080/00986449308936161>
- Zakaria, A. K. M., Asgar, M. A., Eriksson, S.-G., Ahmed, F. U., Yunus, S. M., Delaplane, R. G., Stanciu, V., & Svedlindh, P. (2004). Crystallographic and magnetic properties of the spinel type solid solution Zn_{0.4}Co_{0.6}Al_xFe_{2-x}O₄ (0 ≤ x ≤ 1). *Materials Research Bulletin*, 39(7-8), 1141-1157.
<https://doi.org/10.1016/j.materresbull.2004.02.015>
- Zakaria, A. K. M., Asgar, M. A., Eriksson, S.-G., Ahmed, F. U., Yunus, S. M., & Rundlöf, H. (2003). The study of magnetic ordering in the spinel system Zn_xNi_{1-x}FeCrO₄ by neutron diffraction. *Journal of Magnetism and Magnetic Materials*, 265(3), 311-320.
[https://doi.org/10.1016/S0304-8853\(03\)00280-4](https://doi.org/10.1016/S0304-8853(03)00280-4)
- Zhang, S.-C., Messing, G. L., & Borden, M. (1990). Synthesis of Solid, Spherical Zirconia Particles by Spray Pyrolysis. *Journal of the American Ceramic Society*, 73(1), 61-67.
<https://doi.org/10.1111/j.1151-2916.1990.tb05091.x>

